



## Supporting Online Material for

### **Supracolloidal Reaction Kinetics of Janus Spheres**

Qian Chen, Jonathan K. Whitmer, Shan Jiang, Sung Chul Bae, Erik Luijten, Steve Granick\*

\*To whom correspondence should be addressed. E-mail: sgranick@uiuc.edu

Published 14 January 2011, *Science* **331**, 199 (2011)  
DOI: 10.1126/science.1197451

#### **This PDF file includes:**

Materials and Methods

Figs. S1 to S3

References

#### **Other supplemental material for this manuscript includes the following:**

Movies S1 to S6

## **Method and Materials:**

### **Experiments**

Fluorescent latex particles of sulfate polystyrene (1  $\mu\text{m}$  in diameter, F-8851 from Invitrogen, Inc.) are made hydrophobic on one hemisphere through successive deposition of titanium (2nm) and gold (15 nm) thin films, onto which are formed self-assembled monolayers of *n*-octadecanethiol (Sigma-Aldrich). This process produces spheres which are hydrophobic on one surface region and negatively charged elsewhere. Using epifluorescence microscopy (63 $\times$  air objective with a 1.6 $\times$  or 2.5 $\times$  post magnification, N.A. = 0.75), we track and identify each three-dimensional shape. This allows

visualization of the cluster evolution. The experiments are performed at room temperature in water with additional salt (NaCl).

### Theoretical Methods

The relative free energy of various helical structures (4) as a function of Janus balance (Fig. 3A) is calculated by considering the orientational freedom of a single Janus particle.

This particle  $i$  is taken to be far from the ends of a chain (as particles near the end have considerably more rotational freedom) and all its nearest neighbors  $j$  are fixed with their director perpendicular to the helical axis, their hydrophobic side facing inward. This is a plausible first approximation, since deviations of neighboring particles from their average orientation that would increase the rotational freedom of the central Janus sphere  $i$  would also *decrease* the rotational freedom of other Janus spheres in the helix. The central particle interacts only with its nearest neighbors  $j$  through an angular square well attraction, and only attractive orientations of the particle are permitted,

i.e.,  $\cos^{-1}(\hat{\mathbf{r}}_{ij} \cdot \hat{\mathbf{d}}_i) < \alpha$ . We compute the orientational entropy from a Monte Carlo integral over the corresponding rotational phase space.

Collective distortions of the helix are the next correction to the free-energy difference between 3(0,1,1) and BC helices. We calculate the contribution of vibrational modes to this difference following the approach of Ref. 5, using a representative  $N = 24$  chain length. This involves obtaining the eigenvalues of the Hessian matrix of coordinate derivatives, which yield the spring constants and normal modes associated with each

structure (up to the six zero modes associated with overall translation and rotation). The vibrational partition function for each mode is then

$$Z_m = \int_{-\infty}^{\infty} dq_m e^{-\frac{\lambda_m q_m^2}{2k_B T}} \propto \sqrt{\frac{2\pi}{\lambda_m}}, \quad (1)$$

yielding the free energy per particle,

$$f = -\frac{1}{N} \log \left( \prod_m Z_m \right) = -\frac{1}{N} \log \left( \prod_m \sqrt{\frac{2\pi}{\lambda_m}} \right). \quad (2)$$

Here  $m$  ranges only over the rigid modes, which have nonzero spring constant  $\lambda_m$ . For nonrigid modes, the degrees of freedom must be integrated explicitly (5). Here this is unnecessary, as the two structures considered each have only rigid modes aside from global translation and rotation of the particle aggregate. The vibrational correction reduces the free-energy difference between the BC helix and the 3(0,1,1) helix, although the latter remains the thermodynamically favored state at  $\alpha = 90^\circ$ . The calculation is independent of interaction strength, as the internal energy of all conformations is identical; in reality a change in relative orientation of two Janus spheres may affect their pair energy even when their hydrophobic sides continue to face each other, e.g., because of the change in proximity of their charged hemispheres. This in turn results in spin-wave like modes, a correction that is not considered here.

**Simulation Methods:** Molecular dynamics (MD) simulations are performed in the *NVT* ensemble. Particle positions, velocities, and angular velocities are updated through a velocity-Verlet scheme, where the particle orientations are updated by vector rotation rules. Thermalization is achieved through application of a Langevin thermostat to both the linear and angular degrees of freedom. The colloid mass is set by  $M$ , and the moment

of inertia by  $I$  in accordance with a uniform density distribution within the particles. Energies are expressed in units of  $k_B T$ , and lengths in units of the colloid diameter  $\sigma$ .

The attraction is represented by a potential well of tunable range and strength,

$$\Phi(\mathbf{r}_{12}, \hat{\mathbf{d}}_1, \hat{\mathbf{d}}_2) = \epsilon \left\{ \left( \frac{\sigma}{r_{12}} \right)^{100} + \frac{1}{2} f(\theta_1) f(\theta_2) \right. \\ \left. \times \left[ \tanh \left( 100 \left( 1 + \eta - \frac{r_{12}}{\sigma} \right) \right) - \tanh \left( 100 \left( 1 - \frac{r_{12}}{\sigma} \right) \right) \right] \right\}, \quad (3)$$

where

$$\cos^2 \left( \frac{\pi}{2} \frac{\theta - \alpha - \alpha_{\text{tail}}}{2\alpha_{\text{tail}}} \right). \quad (4)$$

Here  $\alpha$  is the angle determining the extent of the spherical cap (cf. main text),  $\eta$  sets the interaction range, and  $\alpha_{\text{tail}}$  is an angular parameter determining the rate at which the potential switches on and off. The angles  $\theta_i$  are defined via the director and separation vectors as  $\cos^{-1}(\hat{\mathbf{r}}_{ij} \cdot \hat{\mathbf{d}}_i)$ . The angular interaction [Eq. (4)] has been used in recent simulations of Janus nanoparticles (14) and is chosen to be smooth so that it is integrable in MD. Despite the four-dimensional nature of the true pair potential between Janus particles (SI), the simplified potential [Eq. (3)] captures all aspects essential to the structural properties of Janus aggregates. The range  $\eta = 0.02$  is chosen sufficiently small to enforce contact interactions, disfavoring more loosely bound structures that will result for attraction ranges beyond  $\eta \approx 0.05$ . The short interaction range requires a rather small time step  $\Delta t_{\text{MD}}$ , which is chosen such that the conditions

$$\Delta t_{\text{MD}} \ll \eta \sigma \sqrt{\frac{M}{k_{\text{B}}T}}, \quad (5)$$

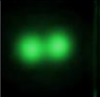
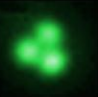

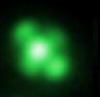

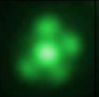
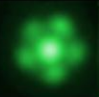
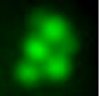







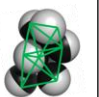
and

$$\Delta t_{\text{MD}} \ll \alpha_{\text{tail}} \sqrt{\frac{I}{k_{\text{B}}T}}, \quad (6)$$

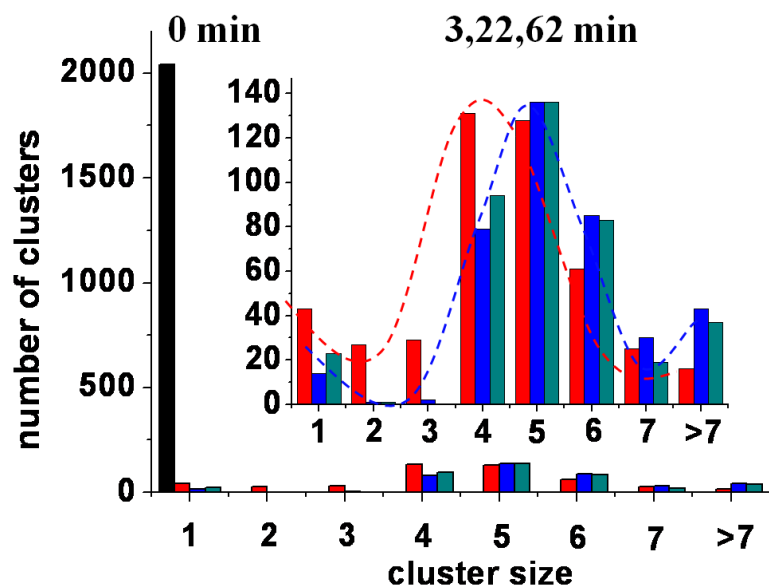
are both satisfied. This ensures proper exploration of the attractive potential well in both the radial and tangential directions. A more stringent condition is that simulations of these conditions in the *NVE* ensemble do not experience significant energy drift. This was verified for a timestep of  $4.6 \times 10^{-5} \sqrt{M\sigma^2 / k_{\text{B}}T}$ . The limited number of particles ( $N = 800$ ) allows exploration of the system over prolonged periods. The attraction strength equals  $0.464043\varepsilon$  for  $\eta = 0.02$ , where  $\varepsilon$  is varied from  $10 k_{\text{B}}T$  to  $40 k_{\text{B}}T$ . The Janus balance is varied over the range  $80^\circ \leq \alpha \leq 90^\circ$ . Attraction strengths of 9.28, 13.9, and  $18.6 k_{\text{B}}T$  are examined, with the tail angle chosen to be  $\alpha_{\text{tail}} = 0.25^\circ$ . Simulations proceed from an initially uniform dispersion of Janus particles in a cell of height  $15\sigma$  that is replicated periodically in the  $x$  and  $y$  directions, whereas the top and bottom walls are represented by shifted-truncated Lennard-Jones potentials. The  $x$  and  $y$  dimensions are equal and chosen to yield a global volume fraction  $\varphi = 0.014$ . A gravitational force  $Mg = 0.54 k_{\text{B}}T/\sigma$  is imposed that causes the particles to sediment collectively while aggregating. After sedimentation, particles occupy a thin layer  $\approx 2\sigma$  in height, yielding effective volume fractions which are increased accordingly (to 10% solid fraction for the systems studied). Structural images are obtained after more than  $5 \times 10^6$  time steps, i.e., more than 100 diffusion times  $\tau_D = \sigma^2/(4D_{\text{self}})$ . In the analysis, the number of tetrahedra

$N_{\text{tetra}}$  each particle occupies (Fig. 3B) is obtained from the frames by checking the  $N$ -particle adjacency matrix of each cluster for four-particle subgraphs of the tetrahedral type. Figures depicting simulation data and helical structures were created using PyMOL (S2).

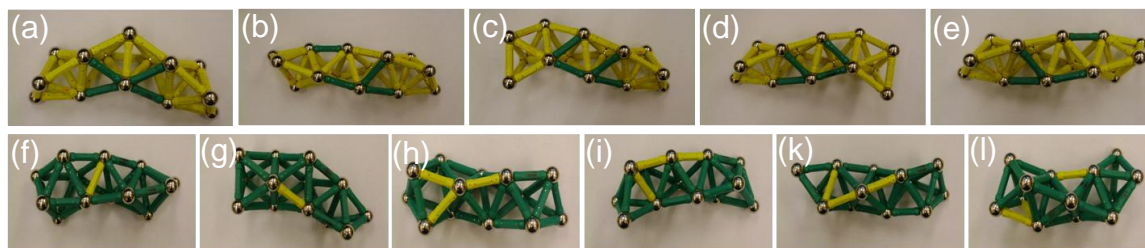
### Supporting Figures and Captions

cluster size	2	3	4	5	6	6	7	7
cluster image								
cluster shape								
# of contacts	1	3	6	9	12	12	15	15

**Fig. S1. Clusters in the reaction network shown in Fig. 1A.** At 3.8 mM NaCl salt, stable small clusters are formed from Janus spheres. Tabulation shows number of particles in the cluster, cluster shape, and number of contacts between hydrophobic patches. Note that per particle, the maximum allowed number of contacts is six.



**Fig. S2. A study of isomerization and equilibration.** Histogram of cluster sizes after initiating the cluster process by adding NaCl to 3.8 mM concentration, evaluated at 0 min (black), 3 min (red), 22 min (blue), and 62 min (green), showing that the size distribution equilibrates after  $\approx 20$  min. Time  $t=0$  is when salt is added.



**Fig. S3: Helical transformation pathway.** The figure above illustrates the possible bond changes around the pivot points with seven nearest neighbors during a chirality [(a)–(e)] or helicity [(f)–(l)] switch. (a) Illustration of the four bonds (green) with reduced stability around a pivot point in a BC helix undergoing chirality change. [(b)–(e)] shows the resulting structures after we break one of the four unstable green bonds, in a



clockwise manner from the bottom left respectively. In each case, the absence of one bond, leaving all other bonds intact, allows relaxation of the two parts originally bridged by the broken bond, until they are locked into place again by a newly formed bond. The result is a propagation of chirality (either forward or backward) along the chain. (f) Illustration of a joint between a 3(0,1,1) helix and a BC helix, and the bond (yellow) which must be broken for the helicity change from BC helix to 3(0,1,1) to progress. (g) The structure after propagation the helicity change through breaking the yellow bond and twisting the two sides into the newly accessible structure. (h) Illustration of the three bonds (yellow) with reduced stability around a pivot point in a 3(0,1,1) helix- BC helix joint. [(i)–(l)] Starting from the left-most and then in a clockwise manner, we break one yellow bond in each case and relax the structure into the new ones afforded by this freedom. None of these cases results in propagation of the new 3(0,1,1) symmetry. (i),(k) result in transformation of the octahedron into face-sharing tetrahedra, while (l) results in rotation of the pivot around the octahedron. All the structures shown in the figure are created using magnetic sticks (CMS Magnetics, Inc.).

### **Supporting References**

- S1. L. Hong, A. Cacciuto, E. Luijten, S. Granick, Clusters of charged Janus spheres. *Nano Lett.* **6**, 2510–2514 (2006).
- S2. The PyMOL molecular graphics system, Version 1.2r3, Schrödinger, LLC. <http://www.pymol.org> (2010).

**Movie S1:** This movie file illustrates a dynamic pathway of sequential cluster growth. A dimer forms into a trimer by addition of one particle. Then the trimer interacts with a tetrahedron nearby, fusing with it to form a chiral heptamer. The heptamer fluctuates and finally evolves to form an octahedral cluster. The movie is acquired at 5 fr/s and is played at 15 fr/s.

**Movie S2:** This movie file shows the isomerization of a chiral heptamer into a symmetric, “flower”-shaped heptamer. A short-lived intermediate cluster is observed during the process. The movie is acquired at 5 fr/s and is played at 15 fr/s.

**Movie S3:** This movie file shows the isomerization of a “flower”-shaped heptamer into a chiral heptamer via the sliding of two neighboring particles. The movie is acquired at 5 fr/s and is played at 15 fr/s.

**Movie S4:** This movie file shows the spontaneous switch of handedness of a chiral chain in experiments. The movie is acquired at 5 fr/s and is played at 10 fr/s.

**Movie S5:** This movie file is an animation showing the bonding topology during switching of handedness of a chiral chain. For this  $N=10$  chiral chain, the change in handedness involves the breaking and formation of one bond.

**Movie S6:** This movie file shows the time-dependent fusion at their ends of two chiral chains with different handedness. The movie is acquired at 5 fr/s and is played at 15 fr/s.